Defect properties and *p*-type doping efficiency in phosphorus-doped ZnO

Woo-Jin Lee, Joongoo Kang, and K. J. Chang
Department of Physics, Korea Advanced Institute of Science and Technology, Daejeon 305-701, Korea
(Received 5 July 2005; revised manuscript received 15 November 2005; published 31 January 2006)

Based on first-principles pseudopotential calculations, we investigated the electronic structure of various P-related defects in ZnO and the *p*-type doping efficiency for two forms of P dopant sources such as P_2O_5 and Zn_3P_2. As compared to N dopants, a substitutional P at an O site has a higher ionization energy of about 0.62 eV, which makes it difficult to achieve *p*-type ZnO. Under Zn-rich growth conditions, P_O acceptors are compensated by dominant donors such as P_{Zn}, leading to *n*-type conduction. Although a P_{Zn}-$2V_{Zn}$ complex, which consists of a substitutional P at a Zn antisite and two Zn vacancies, acts as an acceptor, the formation of Zn vacancies is more probable on going to O-rich conditions for the dopant source using P_2O_5. On the other hand, when Zn_3P_2 is used as the P dopant source, the P_{Zn}-$2V_{Zn}$ complex is energetically more favorable and becomes the dominant acceptor under O-rich growth conditions.

DOI: 10.1103/PhysRevB.73.024117 PACS number(s): 61.72.Bb, 61.72.Vv, 61.72.Ji, 71.55.Gs

As a wide band-gap semiconductor, ZnO has recently attracted much attention because of possible applications for optoelectronic devices such as lasers and light emitting diodes.[1–3] Due to the large exciton binding energy of 60 meV, ZnO is considered as the brightest emitter among the available wide-gap semiconductors even at room temperature. Alloying this material with Mg extends applications to the ultraviolet range.[4,5] Despite other advantages such as the availability of large substrates, high radiation resistance, and low material costs,[6] applications of ZnO are hindered by the difficulty of making reproducible low resistivity *p*-type ZnO.

Nominally undoped ZnO exhibits *n*-type conductivity, which is attributed to the formation of donors such as O vacancies, Zn interstitials, and H impurities. It is now possible to achieve electron densities as high as 10^{21} cm^{-3}.[7] On the other hand, it is known that the fabrication of low resistivity *p*-type ZnO is difficult due to the self-compensation and low solubility of dopants. There have been many attempts to overcome the *p*-type doping problem by using different forms of dopant sources. So far only group-V elements such as N, P, and As have produced low resistivity, *p*-type ZnO, while recent first-principles calculations suggested that the solubility of group-I elements such as Li and Na would be greatly enhanced by hydrogenation, and a subsequent annealing process leads to the activation of passivated acceptors.[8] Among group-V elements, N is used as a popular *p*-type dopant.[9–17] Theoretical studies indicated that the acceptor level of N is so deep that it is difficult to explain the activity of N acceptors at room temperature.[18,19] In addition, it was addressed theoretically that the doping efficiency of N acceptors is limited by the compensation effect by N_2 complexes, which behaves as a double donor.[20] Nevertheless, several experiments have been successful in achieving *p*-type ZnO doped with N impurities, with hole carrier concentrations of about 10^{17}–10^{19} cm^{-3}.[12,15,17] A few reports of *p*-type ZnO have been given for other group-V elements such as P and As.[21–27] Experimental findings of *p*-type conduction in As- and P-doped ZnO are quite puzzling by considering the fact that As_O and P_O acceptors have very high ionization energies due to the large atomic radii of the As and P atoms.[18,19] For As dopants, it was suggested that an As_{Zn}-$2V_{Zn}$ complex, in which the As atom occupying a Zn site gives a shallow acceptor level by forming a complex with two Zn vacancies, would be the origin of *p*-type conduction.[28] In P-doped ZnO, the reproducibility of *p*-type conduction with P_2O_5 as a dopant source was shown to be relatively poor,[21–23] compared with the other dopant source of Zn_3P_2.[24,25] However, the microscopic structure of dominant acceptors in P-doped ZnO is not yet established. Moreover, the difference in doping efficiency between two dopant sources, P_2O_5 and Zn_3P_2, is not clearly understood.

In this paper, we investigated the electronic structure of various defects in P-doped ZnO through first-principles pseudopotential calculations. By comparing the formation energies of P-related defects and intrinsic point defects, we examined the doping efficiency of P dopants. Similar to As dopants, a substitutional P at an O lattice site forms a deep acceptor level due to the increase of the *p*-orbital energy. On the other hand, a substitutional P (P_{Zn}) at a Zn lattice site, which is energetically favorable under Zn-rich growth conditions, behaves as a donor, compensating for acceptors. The most stable structure of a P_{Zn}-$2V_{Zn}$ complex is found to be different from that for the As_{Zn}-$2V_{Zn}$ complex,[28] which was previously proposed to be the shallow acceptor responsible for the *p*-type conductivity observed in As-doped ZnO. We find that the formation energy of a Zn vacancy (V_{Zn}) is greatly reduced on going to O-rich growth conditions, and this acceptor defect is more favorable than the P_{Zn}-$2V_{Zn}$ complex, when P_2O_5 is used as a dopant source. For the dopant source using Zn_3P_2, the P_{Zn}-$2V_{Zn}$ complex becomes the dominant acceptor under O-rich conditions, with the formation energy much lower than for the Zn vacancy.

Our calculations were performed using the first-principles pseudopotential method within the density-functional theory.[29] We employed the generalized gradient approximation (GGA) for the exchange-correlation potential.[30] Ultrasoft pseudopotentials which include the Zn 3*d* states in the valence shell were used, so that *p*-*d* interactions were considered.[31] The wave functions were expanded in plane waves with a cutoff energy of 30 Ry, and the cutoff energy up to 50 Ry was tested to ensure numerical convergence. We

employed a supercell containing 72 host atoms in the wurtzite structure. We estimated the lattice parameter of $a=3.28$ Å and the axial ratio of $c/a=1.60$, in good agreement with the measured values of $a=3.25$ Å and $c/a=1.60$.[32] The summation of the charge densities over the Brillouin zone was done using a k-point set generated by the $2\times2\times2$ Monkhorst-Pack mesh.[33,34] We tested a larger number of k points, such as the $3\times3\times3$ mesh, and found that the total energies for the P_{Zn} and V_{Zn} defects are accurate to within 0.02 eV. Ionic coordinates were fully relaxed until the maximum forces on each atom are less than 0.12 eV/Å.

The formation energy of a defect D is expressed as

$$E_f(D,q) = E_{tot}(D,q) - n_{Zn}\mu_{Zn} - n_O\mu_O - n_P\mu_P + q\mu_e, \quad (1)$$

where $E_{tot}(D,q)$ is the total energy of a supercell containing the defect in charge state q.[35] Here n_i and μ_i are the number of species i (i=Zn, O, and P) in the supercell and the corresponding reservoir chemical potential, respectively, and μ_e is the Fermi level with respect to the valence-band edge. In ZnO, the chemical potentials of Zn and O satisfy the relations, $\mu_{Zn}+\mu_O=\mu_{ZnO}^{bulk}$, $\mu_O \leqslant \mu_{O_2}/2$, and $\mu_{Zn} \leqslant \mu_{Zn}^{metal}$. Growth conditions are described by the stoichiometric parameter λ, which lies between 0 and 1 under extreme Zn- and O-rich conditions, respectively, when μ_{Zn} and μ_O are expressed as $\mu_{Zn}=\mu_{Zn}^{metal}-\lambda\Delta H$ and $\mu_O=\mu_{O_2}/2-(1-\lambda)\Delta H$. In our calculations, we use the calculated value of 2.88 eV for the heat of formation of ZnO, as compared to the experimental value of 3.61 eV.[36] The transition level, $\varepsilon(q/q')$, of a defect is defined as the energy where the formation energies for two charge states, q and q', are crossed. For charged defects, a jellium background was used. In the supercell calculations using periodic boundary conditions, electrostatic interactions between charged defects in different supercells may cause errors on a real aperiodic system with defects, which corresponds to the dilute limit.[37,38] However, previous calculations showed that for defects with delocalized charge distributions such as shallow defects, the Coulomb energy is smaller than what is expected from a point-charge model for defects.[39] Thus we expect that spurious Coulomb interactions between the charged defects in supercells do not significantly affect the formation energies since shallow defects are considered. We calculated the defect energies, which are defined as the difference between the total energies with and without a defect, for 32-, 64-, 72-, and 108-atom supercells, which are shown in Table I, and extracted the formation energies and transition levels of defects in the dilute limit by linearly fitting the defect energies to the inverse of cell volume.[40] For ZnO, the calculated band gap of 1.75 eV is underestimated, as compared to the measured value of 3.44 eV. In calculating the formation energies of donors such as $(P_2)_O$ and P_{Zn}, we included the band-gap correction of 1.69 eV.

First we examined P-related defects involving substitutional P impurities, P_{Zn} and P_O at the Zn and O lattice sites, respectively, and defect complexes such as a P_2 molecule $[(P_2)_O]$ and a P_{Zn}-$2V_{Zn}$ complex which consists of a P dopant at the Zn antisite and two Zn vacancies. The P_O and P_{Zn}-$2V_{Zn}$ defects behave as an acceptor, while the P_{Zn} and $(P_2)_O$ defects act as a donor.

TABLE I. The defect energies (in units of eV) of P_O, V_{Zn}, and P_{Zn}-$2V_{Zn}$, which are given by the difference between the total energies calculated with and without defects, are listed for various supercell sizes. The defect energies for the 72-atom cell are set to be zero.

Defects	32-atom cell	64-atom cell	72-atom cell	108-atom cell
P_O^{1-}	0.556		0	−0.013
P_O	0.045		0	0.019
V_{Zn}^{2-}	−0.567		0	0.291
V_{Zn}^{1-}	−0.339		0	0.110
V_{Zn}	0.073		0	−0.011
$(P_{Zn}\text{-}2V_{Zn})^{2-}$		−0.239	0	0.305
$(P_{Zn}\text{-}2V_{Zn})^{1-}$		−0.199	0	0.412
$P_{Zn}\text{-}2V_{Zn}$		−0.052	0	0.198

For a substitutional P_O acceptor, because of the large size mismatch between the P and O atoms, the Zn-P bond distances are calculated to be 2.23–2.24 Å, which are larger than the calculated Zn-O bond length of 2.00 Å for bulk ZnO. Although the P_O defect acts as a single acceptor, the $(1-/0)$ transition level of this acceptor is located at 0.95 eV above the valence-band maximum (VBM), similar to previous theoretical calculations.[19] Since the p-orbital energy increases as going from N to P, the acceptor transition level of P_O becomes deeper inside the gap, as compared to the transition level of 0.47 eV for the N_O acceptor.[20] To find the $(1-/0)$ transition level in the dilute limit, we tested other 32- and 108-atom supercells, and estimated this transition level to be 0.62 eV above the VBM. Due to the deep transition level, the P_O acceptor is unlikely to be responsible for the p-type conduction observed in P-doped ZnO.

When a P dopant occupies a Zn lattice site [see Fig. 1(a)], this defect behaves as a triple donor. The $(0/1+)$ transition level of P_{Zn} lies above the conduction-band minimum, becoming a shallow donor. Since the atomic radius of P is smaller than that of Zn, the four neighboring O atoms are relaxed towards the P_{Zn} defect. The P_{Zn} donor has two types of P_{Zn}-O bonds due to the hexagonal symmetry: one bond aligned on the c axis, and the other three bonds off the c axis. For the neutral charge state, the P_{Zn}-O bond on the c axis has the bond distance of 1.68 Å, while the bond distances of the *off* bonds are 1.91 Å. When an electron is ionized from the P_{Zn} donor, the bond distances of the *off* bonds are reduced by 0.31 Å, while the *on* bond on the c axis is little affected. From the analysis of the density of states, we noted that the P_{Zn} defect has two additional transition levels, $\varepsilon(1+/2+)$ and $\varepsilon(2+/3+)$. The highest occupied single-particle level of P_{Zn}^+, which is occupied by two electrons, is located just below the conduction-band minimum, and its associated wave function exhibits the antibonding characteristics of the P-O bond, as shown in Fig. 2(a). Since this defect level is conduction-band-like, we expect that the $\varepsilon(1+/2+)$ and $\varepsilon(2+/3+)$ transition levels are close to the conduction-band minimum even if the band-gap correction is included.

In previous calculations for ZnSe and ZnO doped with N impurities, N_2 molecules at the anion lattice sites were

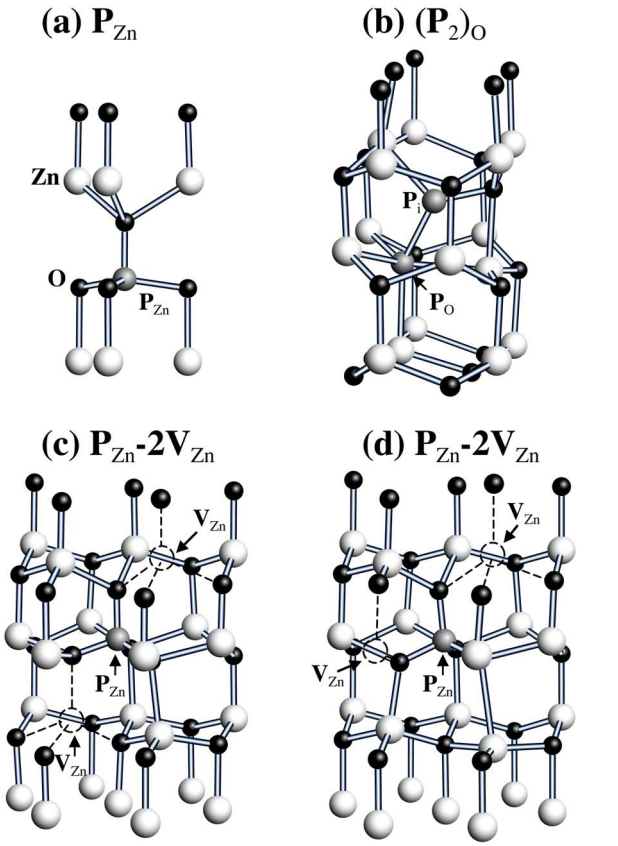

FIG. 1. (Color online) Atomic structures of P-related defects in ZnO: (a) a substitutional P at an Zn lattice site, (b) a $(P_2)_O$ molecule at an O lattice site, and (c) a metastable P_{Zn}-$2V_{Zn}$ isomer, and (d) the most stable P_{Zn}-$2V_{Zn}$ complex.

shown to act as a shallow double donor, which compensates for N acceptors.[20,41] For P dopants in ZnO, we also found a similar $(P_2)_O$ molecule at the O lattice site [see Fig. 1(b)], which effectively consists of a substitutional P at the O site and an interstitial P (P_i). The P-P bond length is calculated to be 2.19 Å for the neutral charge state, which is slightly larger than the calculated value of 1.89 Å for a free P_2 molecule in vacuum, in good agreement with the experimental value of 1.90 Å.[42] Similar to an isolated P_O, the $(P_2)_O$ molecule has the bond lengths of 2.23–2.34 Å between the P_O and its neighboring Zn atoms. The defect level of $(P_2)_O$ lies in the conduction band, indicating that the $(P_2)_O$ molecule acts as a shallow donor. This donor state is mainly characterized by the antibonding $pp\pi^*$ state of the P_2 molecule, as shown in Fig. 2(b), very similar to the $(N_2)_O$ and $(N_2)_{Se}$ molecules in ZnO and ZnSe, respectively. When two electrons are ionized from the $(P_2)_O$ molecule, the P-P bond length is reduced to 2.07 Å due to the loss of the antibonding nature of the donor state. Since the formation of $(P_2)_O$ is accompanied with large lattice relaxations, its energy is higher than that for P_{Zn}. If the $(P_2)_O$ molecule is formed under nonequilibrium condition, annealing will dissociate the interstitial P from the molecule and then activate the acceptor behavior of the substitutional P.

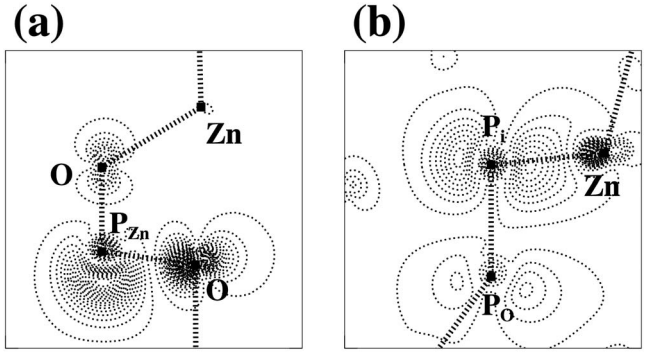

FIG. 2. Charge-density contours for the donor levels of (a) P_{Zn} and (b) $(P_2)_O$, with the contour spacing of 0.002 a.u.

In ZnO doped with dopants such as As and Sb, the As_{Zn}-$2V_{Zn}$ and Sb_{Zn}-$2V_{Zn}$ complexes were suggested to be responsible for *p*-type conduction.[28] Due to a charge transfer of three electrons from the As_{Zn} to two V_{Zn} defects, strong Coulomb interactions between oppositely charged defects lead to a large binding energy. For the neutral and 1- charge states, a fivefold configuration, where the As_{Zn} atom is bonded to five neighboring O atoms, was shown to be more stable than a fourfold structure. For the P_{Zn}-$2V_{Zn}$ complex, there are 13 isomers, which are determined by the positions of two Zn vacancies around the P_{Zn} atom. In this case, we found that the fourfold structure in Fig. 1(c) is more stable by 1.0 eV than the atomic structure with five P-O bonds. As the size of dopant atom decreases, going from Sb to P, the stable structure tends to be the fourfold structure because it costs a large strain energy to form an additional dopant-O bond. Among the isomers, the most stable configuration is shown in Fig. 1(d), and this structure is lower in energy by 0.05–1.37 eV than for other isomers. We estimated the binding energy of 1.38 eV for the formation of the most stable P_{Zn}-$2V_{Zn}$ complex from individual defects via the reaction

$$P_{Zn}^{3+} + 2V_{Zn}^{2-} \rightarrow (P_{Zn} - 2V_{Zn})^{-}. \quad (2)$$

Since this binding energy is smaller than the value of 2.84 eV for the As_{Zn}-$2V_{Zn}$ complex, a strong competition of the P_{Zn}-$2V_{Zn}$ complex with other acceptors such as V_{Zn} may not enhance greatly the concentration of the P_{Zn}-$2V_{Zn}$ complex under high-temperature growth. In the 1-charge state, where the acceptor level is fully occupied, the calculated P-O bond lengths are 1.57–1.60 Å, similar to those for the 3+ charge state of P_{Zn}. In the dilute limit, the $\varepsilon(1-/0)$ transition level is found to lie at 0.55 eV above the VBM, indicating a rather deep acceptor, while those for the $\varepsilon(2-/1-)$ and $\varepsilon(3-/2-)$ transitions are located at 2.79 eV above the VBM and in the conduction band, respectively.

Among native defects, O and Zn vacancies were mostly studied in previous theoretical calculations.[20,43,44] The wave function of the V_O defect level is mainly composed of the Zn 4*s* and O 2*p* orbitals. The V_O defect was considered as the main source of intrinsic *n*-type conduction. Our calculations showed that the V_O defect behaves as a negative-*U* defect, with the (0/2+) transition level within the gap, in good agreement with other calculations.[43] In our finite-sized-supercell calculations, although V_{Zn} acts as a double acceptor, the transition levels are found to lie within the valence

TABLE II. The formation energies (E_f) of P-related defects and native defects calculated for the 72-atom supercell are listed for the P_4O_{10} molecular source. The formation energies (corrected E_f) estimated in the dilute limit are also given for acceptors such as P_O, P_{Zn}-$2V_{Zn}$, and V_{Zn}, while for $(P_2)_O$ and P_{Zn} donors, the band-gap correction of 1.69 eV is included in their formation energies. The extreme Zn- and O-rich conditions correspond to $\lambda=0$ and 1, respectively, and the zero of μ_e is set to be the top of the valence band.

Defect	E_f (eV)	Corrected E_f (eV)
$(P_2)_O^{2+}$	$16.51-6(1-\lambda)\Delta H+2\mu_e$	$16.51-6(1-\lambda)\Delta H+2\mu_e$
$(P_2)_O^{1+}$	$18.42-6(1-\lambda)\Delta H+\mu_e$	$20.11-6(1-\lambda)\Delta H+\mu_e$
$(P_2)_O$	$20.17-6(1-\lambda)\Delta H$	$23.54-6(1-\lambda)\Delta H$
P_{Zn}^{3+}	$-0.92-\frac{3}{2}(1-\lambda)\Delta H+3\mu_e$	$-0.92-\frac{3}{2}(1-\lambda)\Delta H+3\mu_e$
P_{Zn}^{2+}	$0.75-\frac{3}{2}(1-\lambda)\Delta H+2\mu_e$	$2.44-\frac{3}{2}(1-\lambda)\Delta H+2\mu_e$
P_{Zn}^{1+}	$2.92-\frac{3}{2}(1-\lambda)\Delta H+\mu_e$	$6.30-\frac{3}{2}(1-\lambda)\Delta H+\mu_e$
P_{Zn}	$6.47-\frac{3}{2}(1-\lambda)\Delta H$	$11.54-\frac{3}{2}(1-\lambda)\Delta H$
V_O^{2+}	$1.84-(1-\lambda)\Delta H+2\mu_e$	$1.84-(1-\lambda)\Delta H+2\mu_e$
V_O^{1+}	$3.18-(1-\lambda)\Delta H+\mu_e$	$4.87-(1-\lambda)\Delta H+\mu_e$
V_O	$3.83-(1-\lambda)\Delta H$	$7.21-(1-\lambda)\Delta H$
P_O^{1-}	$12.48-\frac{7}{2}(1-\lambda)\Delta H-\mu_e$	$12.16-\frac{7}{2}(1-\lambda)\Delta H-\mu_e$
P_O	$11.53-\frac{7}{2}(1-\lambda)\Delta H$	$11.54-\frac{7}{2}(1-\lambda)\Delta H$
V_{Zn}^{2-}	$5.01-\lambda\Delta H-2\mu_e$	$5.59-\lambda\Delta H-2\mu_e$
V_{Zn}^{1-}	$5.03-\lambda\Delta H-\mu_e$	$5.32-\lambda\Delta H-\mu_e$
V_{Zn}	$5.28-\lambda\Delta H$	$5.23-\lambda\Delta H$
$(P_{Zn}\text{-}2V_{Zn})^{2-}$	$4.59-\frac{1}{2}\lambda\Delta H-2\mu_e$	$7.35-\frac{1}{2}\lambda\Delta H-2\mu_e$
$(P_{Zn}\text{-}2V_{Zn})^{1-}$	$3.27-\frac{1}{2}\lambda\Delta H-\mu_e$	$4.56-\frac{1}{2}\lambda\Delta H-\mu_e$
P_{Zn}-$2V_{Zn}$	$3.64-\frac{1}{2}\lambda\Delta H$	$4.01-\frac{1}{2}\lambda\Delta H$

band. The underestimation of these transition energies is mainly caused by a large dispersion of the defect level due to the use of a finite-sized-supercell and an upward shift of the valence-band edge due to a *p-d* repulsion generated by including the Zn 3*d* orbitals in the valence shell. In the dilute limit, the transition levels of V_{Zn} are located at $\varepsilon(1-/0)=0.09$ eV and $\varepsilon(2-/1-)=0.27$ eV above the VBM, similar to previous calculations.[20,28]

The formation energies of defects vary with the P chemical potential via Eq. (1), and μ_P depends on the type of dopant sources. Experimentally, two dopant sources such as P_2O_5 and Zn_3P_2 were used to achieve *p*-type conduction in ZnO.[21–25] Under normal conditions of temperature and pressure, the P_2O_5 crystal exists in three different phases: two stable orthorhombic structures which consist of a network of PO_4 tetrahedra and a metastable hexagonal form which is made of discrete P_4O_{10} molecules.[45,46] To determine the maximum value of μ_P, we considered the two orthorhombic phases as well as a P_4O_{10} molecule, which is likely to be formed at high temperatures. For the orthorhombic and layered bulk structures of P_2O_5, their total energies are found to be higher by 0.26 and 0.18 eV, respectively, per unit formula than for the P_4O_{10} molecule. Because the P_4O_{10} molecule is more stable than other phases, we used this molecule as the P_2O_5 dopant source. In this case, the maximum P chemical potential is written as $\mu_P^{max}=\frac{1}{4}\mu_{P_4O_{10}}-\frac{10}{4}\mu_O$, where $\mu_{P_4O_{10}}$ is the total energy of the P_4O_{10} molecule.

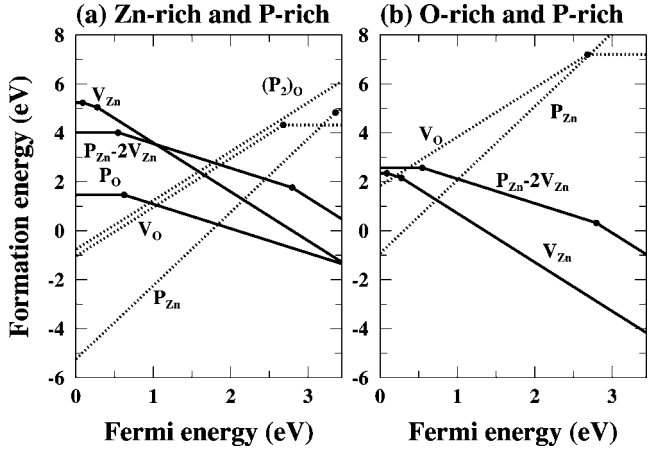

FIG. 3. For the dopant source using a P_4O_{10} molecule, the calculated formation energies of various donors (dotted lines) and acceptors (solid lines) under (a) Zn- and P-rich conditions are drawn as a function of the Fermi energy and compared with those for (b) O- and P-rich conditions. For acceptors such as P_O, P_{Zn}-$2V_{Zn}$, and V_{Zn}, the formation energies are estimated in the dilute limit, and for $(P_2)_O$ and P_{Zn} donors, their formation energies include the band-gap correction.

For the dopant source of the P_4O_{10} molecule, the formation energies of P-related defects and point defects are listed under the P-rich condition ($\mu_P=\mu_P^{max}$) in Table II. In the dilute limit, the formation energies of defects are plotted as a function of the Fermi energy under the Zn- and O-rich conditions in Fig. 3. Under the Zn- and P-rich conditions, the P_O acceptor is more stable than the other acceptors such as V_{Zn} and P_{Zn}-$2V_{Zn}$ for the Fermi level near the VBM. However, the P_O acceptors are mostly compensated by the triple P_{Zn} donors, which have the lower formation energy. Due to the dominant P_{Zn} donors, it will be difficult to obtain *p*-type conduction. Recent experiments showed that with P_2O_5 as the dopant source, as-grown epitaxial ZnO films are highly conductive and *n*-type.[22,23] Since ZnO films were grown with large P contents of 1–5 at. %, the observed *n*-type conduction may be attributed to the formation of the P_{Zn} donor. If the P_{Zn} donor is inhibited by any means, *p*-type conduction would be possible by the P_O acceptors. As going to the O-rich condition, the formation energies of the acceptors involving V_{Zn} are lowered, while those for the other defects such as P_O, P_{Zn}, and V_O increase. Since the energy lowering of V_{Zn} is larger than for the P_{Zn}-$2V_{Zn}$ complex, V_{Zn} becomes a major acceptor, as shown in Fig. 3(b). Although the P_{Zn} defect is still the most favorable donor, *p*-type conduction is likely to occur due to the V_{Zn} defect. If a P_4O_6 molecule is considered as the dopant source, this molecule has a higher value of μ_P^{max} by 2.78 eV than for the P_4O_{10} molecule. In this case, since the formation energy of P_{Zn}-$2V_{Zn}$ is lowered, the P_{Zn}-$2V_{Zn}$ complex becomes the dominant acceptor.

When Zn_3P_2 is used as the dopant source, the value of μ_P^{max} is determined by the relation, $\mu_P^{max}=\frac{1}{2}\mu_{Zn_3P_2}^{bulk}-\frac{3}{2}\mu_{Zn}$, where $\mu_{Zn_3P_2}^{bulk}$ is the total energy of bulk Zn_3P_2 per unit formula. Figure 4 shows the formation energies of various de-

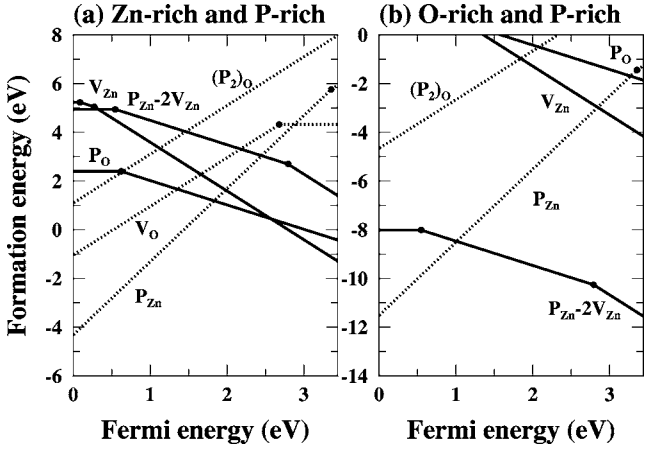

FIG. 4. For the dopant source using Zn_3P_2, the calculated formation energies of various donors (dotted lines) and acceptors (solid lines) under (a) Zn- and P-rich conditions are drawn as a function of the Fermi energy and compared with those for (b) O- and P-rich conditions. For acceptors such as P_O, P_{Zn}-2V_{Zn}, and V_{Zn}, the formation energies are estimated in the dilute limit, and for $(P_2)_O$ and P_{Zn} donors, their formation energies include the band-gap correction.

fects as a function of the Fermi energy under the Zn- and O-rich conditions. Under the Zn- and P-rich conditions, the formation energies of P-related defects such as P_O, $(P_2)_O$, P_{Zn}, and P_{Zn}-2V_{Zn} are enhanced, compared with the P_4O_{10} molecular source in Fig. 3(a). The general feature for the dominant donor and acceptor remains almost unchanged. On the other hand, under the O- and P-rich conditions, the formation energies of P_{Zn} and P_{Zn}-2V_{Zn} are lowered by about 10 eV, while the energy of V_{Zn} is not affected. Thus the P_{Zn}-2V_{Zn} complex becomes a more stable acceptor than for the V_{Zn} defect, as shown in Fig. 4(b). However, a significant increase of hole carrier concentrations is not expected due to the compensation effect by the P_{Zn} donor.

Under thermodynamic equilibrium, the concentration of a defect at temperature T is written as

$$C(D,q) = z_D N_S \exp[-E_f(D,q)/k_B T], \tag{3}$$

where $E_f(D,q)$ is the defect formation energy, N_S is the number of sites where the defect D can be formed per unit volume, and z_D is the number of distinct configurations per sublattice site for a defect complex.[35] The equilibrium Fermi level is determined by the charge neutrality condition,[35] and the total concentration of dopants can be controlled by varying the parameter λ and the dopant chemical potential μ_P. At a growth temperature of 600 °C, the equilibrium Fermi level is found to be around 0.73 eV above the valence-band edge under the O- and P-rich conditions for the P_2O_5 source. The total concentration of P dopants varies from $\sim 10^{15}$ to $\sim 10^{20}$ cm^{-3} as the growth condition changes from the extreme O-rich ($\lambda=1$) to Zn-rich ($\lambda=0$). In the extreme P-rich and O-rich conditions, the concentration of hole carriers is estimated to be in the range of 10^{15} cm^{-3}. When the P_4O_6 molecule is considered as the dopant source, since the formation energies of P-related defects are reduced, the solubility of P dopants increases by two orders of magnitude under P-rich conditions. However, the concentration of hole carriers is expected not to be much enhanced because of the compensation effect by the P_{Zn} donor. For the Zn_3P_2 dopant source, the solubility of P dopants can reach 10^{20} cm^{-3} under the Zn- and P-rich conditions.

In conclusion, we have investigated the electronic structure of P-related defects and the doping efficiency of P dopants in ZnO through the first-principles pseudopotential calculations. We found that the most stable structure of the P_{Zn}-2V_{Zn} complex is different from that previously proposed for the As_{Zn}-2V_{Zn} complex, and the stability of this complex is enhanced under O-rich conditions, where the Zn vacancies are abundant. For the two forms of dopant sources, P_2O_5 and Zn_3P_2, we found that *p*-type ZnO is achievable under O-rich conditions. For the P_2O_5 source, the dominant acceptors are suggested to be the V_{Zn} defects, while the P_{Zn}-2V_{Zn} complex is energetically more favorable for the Zn_3P_2 source.

This work was supported by the Korea Ministry of Commerce, Industry, and Energy.

[1] D. M. Bagnall, Y. F. Chen, Z. Zhu, T. Yao, S. Koyama, M. Y. Shen, and T. Goto, Appl. Phys. Lett. **70**, 2230 (1997).
[2] Z. K. Tang, G. K. L. Wong, P. Yu, M. Kawasaki, A. Ohtomo, H. Koinuma, and Y. Segawa, Appl. Phys. Lett. **72**, 3270 (1998).
[3] D. K. Hwang, S.-H. Kang, J.-H. Lim, E.-J. Yang, J.-Y. Oh, J.-H. Yang, and S.-J. Park, Appl. Phys. Lett. **86**, 222101 (2005).
[4] A. Ohtomo, M. Kawasaki, T. Koida, K. Masubushi, H. Koinuma, Y. Sakurai, Y. Yoshida, T. Yasuda, and Y. Segawa, Appl. Phys. Lett. **72**, 2466 (1998).
[5] T. Makino, Y. Segawa, M. Kawasaki, A. Ohtomo, R. Shiroki, K. Tamura, T. Yasuda, and H. Koinuma, Appl. Phys. Lett. **78**, 1237 (2001).
[6] D. C. Look, Mater. Sci. Eng., B **80**, 383 (2001).
[7] T. Minami, H. Sato, H. Nanto, and S. Takata, Jpn. J. Appl. Phys., Part 2 **24**, L781 (1985).
[8] E.-C. Lee and K. J. Chang, Phys. Rev. B **70**, 115210 (2004).
[9] Y. Sato and S. Sato, Thin Solid Films **281-282**, 445 (1996).
[10] K. Iwata, P. Fons, A. Yamada, K. Matsubara, and S. Niki, J. Cryst. Growth **209**, 526 (2000).
[11] M. Joseph, H. Tabata, and T. Kawai, Jpn. J. Appl. Phys., Part 2 **38**, L1205 (1999).
[12] X.-L. Guo, H. Tabata, and T. Kawai, J. Cryst. Growth **223**, 135 (2001).
[13] K. Minegishi, Y. Koiwai, Y. Kikuchi, K. Yano, M. Kasuga, and A. Shimizu, Jpn. J. Appl. Phys., Part 2 **36**, L1453 (1997).
[14] K. Nakahara, H. Takasu, P. Fons, A. Yamada, K. Iwata, K. Matsubara, R. Hunger, and S. Niki, Appl. Phys. Lett. **79**, 4139 (2001).
[15] D. C. Look, D. C. Reynolds, C. W. Litton, R. L. Jones, D. B. Eason, and G. Cantwell, Appl. Phys. Lett. **81**, 1830 (2002).

[16] A. V. Singh, R. M. Mehra, A. Wakahara, and A. Yoshida, J. Appl. Phys. **93**, 396 (2003).
[17] J. M. Bian, X. M. Li, C. Y. Zhang, W. D. Yu, and X. D. Gao, Appl. Phys. Lett. **85**, 4070 (2004).
[18] A. Kobayashi, O. F. Sankey, and J. D. Dow, Phys. Rev. B **28**, 946 (1983).
[19] C. H. Park, S. B. Zhang, and S.-H. Wei, Phys. Rev. B **66**, 073202 (2002).
[20] E.-C. Lee, Y.-S. Kim, Y.-G. Jin, and K. J. Chang, Phys. Rev. B **64**, 085120 (2001).
[21] K.-K. Kim, H.-S. Kim, D.-K. Hwang, J.-H. Lim, and S.-J. Park, Appl. Phys. Lett. **83**, 63 (2003).
[22] Y. W. Heo, S. J. Park, K. Ip, S. J. Pearton, and D. P. Norton, Appl. Phys. Lett. **83**, 1128 (2003).
[23] Y. W. Heo, K. Ip, S. J. Park, S. J. Pearton, and D. P. Norton, Appl. Phys. A: Mater. Sci. Process. **78**, 53 (2004).
[24] K.-H. Bang, D.-K. Hwang, M.-C. Park, Y.-D. Ko, I. Yun, and J.-M. Myung, Appl. Surf. Sci. **210**, 177 (2003).
[25] T. Aoki, Y. Hatanaka, and D. C. Look, Appl. Phys. Lett. **76**, 3257 (2000).
[26] Y. R. Ryu, S. Zhu, D. C. Look, J. M. Wrobel, H. M. Jeong, and H. W. White, J. Cryst. Growth **216**, 330 (2000); Y. R. Ryu, T. S. Lee, and H. W. White, Appl. Phys. Lett. **83**, 87 (2003).
[27] D. C. Look, G. M. Renlund, R. H. Burgener II, and J. R. Sizelove, Appl. Phys. Lett. **85**, 5269 (2004).
[28] S. Limpijumnong, S. B. Zhang, S.-H. Wei, and C. H. Park, Phys. Rev. Lett. **92**, 155504 (2004).
[29] P. Hohenberg and W. Kohn, Phys. Rev. **136**, B864 (1964); W. Kohn and L. J. Sham, Phys. Rev. **140**, A1133 (1965).
[30] J. P. Perdew and Y. Wang, Phys. Rev. B **45**, 13244 (1992).
[31] D. Vanderbilt, Phys. Rev. B **41**, R7892 (1990).
[32] D. Vogel, P. Krüger, and J. Pollmann, Phys. Rev. B **52**, R14316 (1995).
[33] H. J. Monkhorst, and J. D. Pack, Phys. Rev. B **13**, 5188 (1976).
[34] J. D. Pack, and H. J. Monkhorst, Phys. Rev. B **16**, 1748 (1977).
[35] J. E. Northrup and S. B. Zhang, Phys. Rev. B **47**, R6791 (1993).
[36] *Handbook of Chemistry and Physics*, 73 ed., edited by D. R. Lide (CRC, Boca Raton, FL, 1992).
[37] C. W. M. Castleton and S. Mirbt, Phys. Rev. B **70**, 195202 (2004).
[38] G. Makov and M. C. Payne, Phys. Rev. B **51**, 4014 (1995).
[39] S.-H. Wei, Comput. Mater. Sci. **30**, 337 (2004).
[40] For various defects considered here, the defect energies calculated for the 72-atom supercell vary by 0.01–1.3 eV in the dilute limit. Comparing the optimized geometries for the 72- and 108-atom supercells, we found that the P-O bond lengths change by 0.09–0.2 % for P_O, the O-O bond lengths near V_{Zn} by 0.5–0.9 % for V_{Zn}, and the O-O and P-O bond lengths near V_{Zn} by 0.6–2.6 and 0.5–0.6 %, respectively, for $P_{Zn}-2V_{Zn}$.
[41] B.-H. Cheong, C. H. Park, and K. J. Chang, Phys. Rev. B **51**, 10610 (1995).
[42] V. Wazer, *Phosphorus and Its Compounds* (Interscience, New York, 1958).
[43] A. F. Kohan, G. Ceder, D. Morgan, and Chris G. Van de Walle, Phys. Rev. B **61**, 15019 (2000).
[44] S. B. Zhang, S.-H. Wei, and A. Zunger, Phys. Rev. B **63**, 075205 (2001).
[45] E. H. Arbib, B. Elouadi, J. P. Chaminade, and J. Darriet, J. Solid State Chem. **127**, 350 (1996).
[46] D. W. J. Cruickchank, Acta Crystallogr. **17**, 677 (1964).